Bull. Mater. Sci. (2022) 45:145
https://doi.org/10.1007/s12034-022-02709-1

Ternary CTAB@Co_3O_4@GO nanocomposite as a promising superoxide dismutase mimic

VAISHALI GARG[1], MANPREET KAUR[1,*], MANJEET KAUR SANGHA[2] and MOHAMMED JAVED[3]

[1]Department of Chemistry, Punjab Agricultural University, Ludhiana 141004, India
[2]Department of Biochemistry, Punjab Agricultural University, Ludhiana 141004, India
[3]Department of Mathematics Statistic and Physics, Punjab Agricultural University, Ludhiana 141004, India
*Author for correspondence (manpreetchem@pau.edu)

MS received 11 November 2021; accepted 11 March 2022

Abstract. In the present study, nanocomposite (NC) of cetyl trimethyl ammonium bromide (CTAB) coated cobalt oxide nanoparticles (Co_3O_4 NPs) with graphene oxide (GO), i.e., CTAB@Co_3O_4@GO, was synthesized for superoxide dismutase mimic (SOD) activity. The NPs and NC were characterized using various analytical tools. X-ray diffraction patterns, Fourier transform infrared and scanning electron microscope–energy dispersive spectrum confirmed the presence of both GO and Co_3O_4 NPs in NC. Transmission electron microscope micrographs of NC showed GO nanosheets having CTAB-coated Co_3O_4 NPs on their surface. The NC was evaluated for SOD mimic activity using pyrogallol as a substrate. NC displayed maximum activity as compared to pristine GO and Co_3O_4 NPs. The results signified that the surfactant coating and embedding the NPs in the GO matrix helped in increasing the interaction of NC with the substrate molecules. Kinetics data was modelled using Michaelis–Menton equation. The calculated K_m and V_{max} values of NC were 0.0675 mM and 0.146 mol s^{-1}, respectively. Lower value of Michaelis constant K_m as compared to the reported values, confirm its edge over other SOD mimics. Thus CTAB@Co_3O_4@GO NC holds potential for replacing natural enzyme in SOD-based enzymatic assay.

Keywords. Superoxide dismutase mimic; Co_3O_4 nanoparticles; CTAB@Co_3O_4@GO; enzyme mimic study.

1. Introduction

Enzymes catalyse various biological reactions and are important for the normal functioning of living beings. Many reactive oxygen species (ROS) are generated during metabolic reactions in the living beings. Superoxide dismutase (SOD) enzyme catalyses the conversion of superoxide anion radicals into relatively less toxic hydrogen peroxide and molecular oxygen. It is a major antioxidant enzyme and exists in all types of living organisms. These ROS are main cause of many chronic diseases like cancer, diabetes and pulmonary diseases. SOD plays pivotal role to defend the body against these diseases. However, like other natural occurring enzymes, it has certain limitations. For the industrial purpose SOD has short life span, works under only low temperature conditions and needs optimum pH conditions. Moreover, it has high cost of production at industrial level. SODs have been used in the clinical trials as they have beneficial effects as antioxidants in the oxidative stress conditions. Major disadvantages that restrict applications of the SOD in therapeutics include their cost, immunogenicity, short life span added to poor cellular accessibility and difficulty in preserving SODs in a biological environment [1]. These constraints can be overcome by using low-molecular-weight complexes mimicking the catalytic activity of SODs, also called SOD mimics [2]. Different SOD mimics have been tested outside of any cellular conditions [3]. Chemistry related to their activity is known as Biomimetic Chemistry. They possess more tunable structures, have high tolerance to environmental conditions and low cost of production. Some artificial enzyme mimics have catalytic and binding sites similar to those of natural enzymes. Iron phosphate microflowers and bioinspired Mn (II) were also used as promising SOD mimics [4].

Cerium vanadate nano enzyme showed SOD mimic activity and has potential application in curing various therapeutic diseases, as these nano enzymes can regulate ATP levels in the cells [5]. Silver NPs were used for antibacterial activity and Selenium NPs for bone tumour therapy by Nikolopoulou *et al* [6] and Barbanente *et al* [7]. Nanoparticles (NPs) can also act as natural enzymes and known as nanozymes. The catalytic activity can be

Supplementary Information: The online version contains supplementary material at https://doi.org/10.1007/s12034-022-02709-1.

Published online: 26 July 2022

maintained, over a wide range of temperature and pH values. Many typical enzymatic reactions mimicking oxidase, peroxidase, lactase, SOD and catalase enzymes have been realized by simple metal and metal oxide NPs, viz. Fe_3O_4, SiO_2, Fe_2O_3, Co_3O_4, CeO_2, FeNi, etc. [8–10]. Cu^{2+} modified covalent triazene framework [11] has also been investigated as enzyme mimic. Nanoceria were the first NPs that were discovered as SOD mimic. Ceria NPs with higher Ce^{3+}/Ce^{4+} ratio were reported to possess higher SOD mimic activity [12]. These existed in the trivalent state (+3) and tetravalent (+4) state, which may flip-flop during redox reaction. Co_3O_4 NPs showed pH-dependent multienzyme activity [13]. In the alkaline and neutral conditions, Co_3O_4 NPs acted as catalase and SOD mimics, whereas in the acidic conditions as peroxidase mimic. Co_3O_4 NPs acted better enzyme mimics, as compared to Fe_3O_4 NPs. An immune histochemical assay also proved that Co_3O_4 NPs could be used as peroxidase mimic.

Discovery of graphene has grabbed attention of researchers to explicate it as enzyme mimic. Graphene is a two-dimensional building block of carbon allotropes. Graphene oxide (GO) is formed by oxidation of graphene employing different methods such as Hummer's, modified Hummer's methods, etc. GO has been used in biosensing [14] and catalysis [15], as it enhances the catalytic activity of metal oxide NPs. GO and Fe_2O_3 nanocomposites (NCs) show π–π interactions with substrate. These interactions increase the adsorption of substrate and its enrichment around NPs, due to which GO and metal oxide composites are better than pristine NPs. Fe_3O_4@-Cu@Cu_2O NC is reported as magnetically recyclable peroxidase mimic [16]. Higher adsorption capability of GO is an advantage for peroxidase and catalase mimic activity [17,18]. Mn_3O_4 nanoflowers have been reported to show SOD, catalase and glutathione peroxidase mimic activity [19]. $Ce_2(MoO_4)_3$/rGO NC were employed for H_2O_2 sensing by Singh *et al* [20]. MnO NPs showing SOD-mimicking activity improved with catechol-PEG, which was used in tumour diagnosis due to its disproportionation mechanism [21]. Copper complexes are reported to show SOD mimic activity [22]. Electrons shuttle between Cu (I) and Cu (II). However, Cu ions are toxic due to which these could not be used in pharmaceutical applications.

The applications of NPs pose a great challenge due to their aggregation and instability. Various stabilizers viz. sodium dodecyl sulphate (SDS), cetyltrimethylammonium bromide (CTAB), octadecyl trichlorosilane (OTS) and long-chain thiols have been widely used as stabilizers, to avoid their aggregation [23,24]. In this work, the two strategies of surfactant coating on Co_3O_4 NPs and nanofabrication with GO were combined. Morphological and structural analysis was done by using various techniques. Effect of CTAB coating and nanofabrication with GO was systematically analysed. Steady-state kinetics of the reaction was studied.

2. Experimental

2.1 *Chemicals used*

All chemicals used viz, cetyl trimethyl ammonium bromide ($C_{19}H_{42}BrN$), cobalt nitrate hexahydrate ($Co(NO_3)_2{\cdot}6H_2O$, ammonia solution 30% ethylenediaminetetra acetate disodium ($C_{10}H_{14}N_2Na_2O_8$), graphite powder, hydrochloric acid (HCl), potassium permanganate ($KMnO_4$), pyrogallol ($C_6H_3(OH)_3$), sodium nitrate ($NaNO_3$), sulphuric acid (H_2SO_4), anhydrous citric acid ($C_6H_8O_7$) were of analytical grade.

2.2 *Synthesis of Co_3O_4 and CTAB-coated Co_3O_4 NPs*

CTAB@Co_3O_4 NPs were prepared by sonication method. CTAB was added in different amounts varying from 0.025–0.1 M (details in scheme 1 and supplementary information) and CTAB-coated Co_3O_4 NPs were labelled as N1, N2 and N3. Ammonia solution (30%) was used to maintain the pH between 8.0 and 9.0. After few hours, a viscous gel was formed and was heated overnight in an oven at 100°C. The precipitates were calcined in the muffle furnace for 3 h at 300°C. Black coloured CTAB-coated Co_3O_4 NPs were obtained and were washed with distilled water and stored in a desiccator. Co_3O_4 NPs were prepared by sol–gel method using citric acid as a complexing agent (see supplementary information for details).

2.3 *Synthesis of CTAB@Co_3O_4@GO NC*

CTAB@Co_3O_4@GO NC was prepared by ultrasonication method [25]. A quantity of 1.0 g of GO and 0.5 g of CTAB-coated Co_3O_4 were mixed in 20 ml of distilled water. The solution was sonicated for 1 h at 25°C followed by filtration and washings with distilled water. The precipitates were dried in oven at 70°C and stored in a vacuum desiccator. Modified Hummer's method was used for the synthesis of GO. Details are given in scheme 2 and in supplementary information.

2.4 *Enzymatic studies*

Enzyme mimic activity of synthesized NPs/NC was studied employing modified Marklund and Marklund method [26]. Pyrogallol (2 ml) of 10 mM concentration and 10 mM of EDTA disodium for reference reading were used. The mixture for enzyme assay was scanned in UV–Visible spectrophotometer typically from 100–600 nm to determine the maximum absorption wavelength (λ_{max}), and it was observed to be 315 nm. This peak corresponded to the oxidized product (scheme 3). Absorbance is inversely proportional to SOD mimic

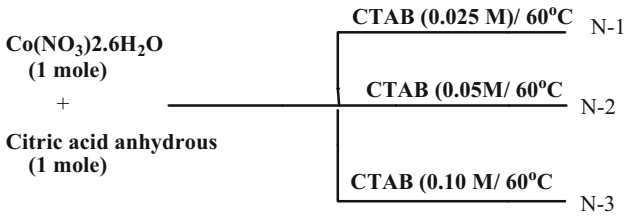

Scheme 1. Molar ratios of CTAB for synthesis of CTAB@Co_3O_4.

activity. Reaction mixture in the absence of NPs was used as control. Percent inhibition of oxidation of pyrogallol in comparison with control was recorded. It was expressed as activity units (A.U.). A 50% inhibition of pyrogallol autooxidation was taken as one A.U. Thus, with an increase in absorbance, decreased value of dismutation was observed, which led to lower SOD mimic activity in activity units. The activities of NPs/NC/GO were evaluated and various parameters viz. pH, temperature, contact time, substrate concentration and NPs dose were optimized. pH was adjusted using 0.1 N HCl and 0.1 N NaOH. The solution was incubated at 25°C. Influence of temperature (10–40°C) was analysed using 2 ml (10 mM) solution of pyrogallol and 1 ml (10 mM) of EDTA disodium solution at optimized pH. To the preceding solution NPs/NC/GO were added. Then solutions were incubated at different temperatures from 10–40°C. Effect of substrate concentration was carried out using 2 ml pyrogallol solution with varying concentrations from 2–40 mM. An aliquot of 1 ml (10 mM) of EDTA disodium solution was added in it, followed by 5 mg of synthesized NPs/NC/GO. Variance in the absorbance was recorded. Effect of NPs dose was evaluated using pyrogallol and EDTA disodium solution in cuvette as described earlier. NPs with varing doses (2–10 mg) were added to 3 ml of substrate solution and change in absorbance was noted. Impact of contact time was recorded by similar reaction mixture containing 5 mg of the NPs. Variation in absorbance was noted up to 150 s at the interval of 30 s. Impact of substrate dose was analysed by varying the pyrogallol concentration (2–10 mM) with 5 mg of NC in it. Reaction system was observed for 150 s and then the data were fitted in Michelis–Menton equation to obtain lineweaver–Burk plot. The slope and intercept of the graph (figure 10) corresponded to $\frac{Km}{Vmax}$ and V_{max}. Michaelis–Menton equation of lineweaver–Burk plot for enzyme catalysed reaction is given below:

$$\frac{1}{v} = \frac{K_m}{V_{max}}\frac{1}{[S]} + \frac{1}{Vmax},$$

where v is initial velocity, V_{max} and $[S]$ are the maximum velocity for reaction and substrate concentration, respectively. K_m is Michaelis–Menten constant, which represents affinity of enzyme for its substrate. Lineweaver–Burk plot of $\frac{1}{[S]}$ *vs.* $\frac{1}{v}$ was used for calculation of K_m and V_{max}. The results of enzymatic studies were analysed statistically by one-way analysis of variance test.

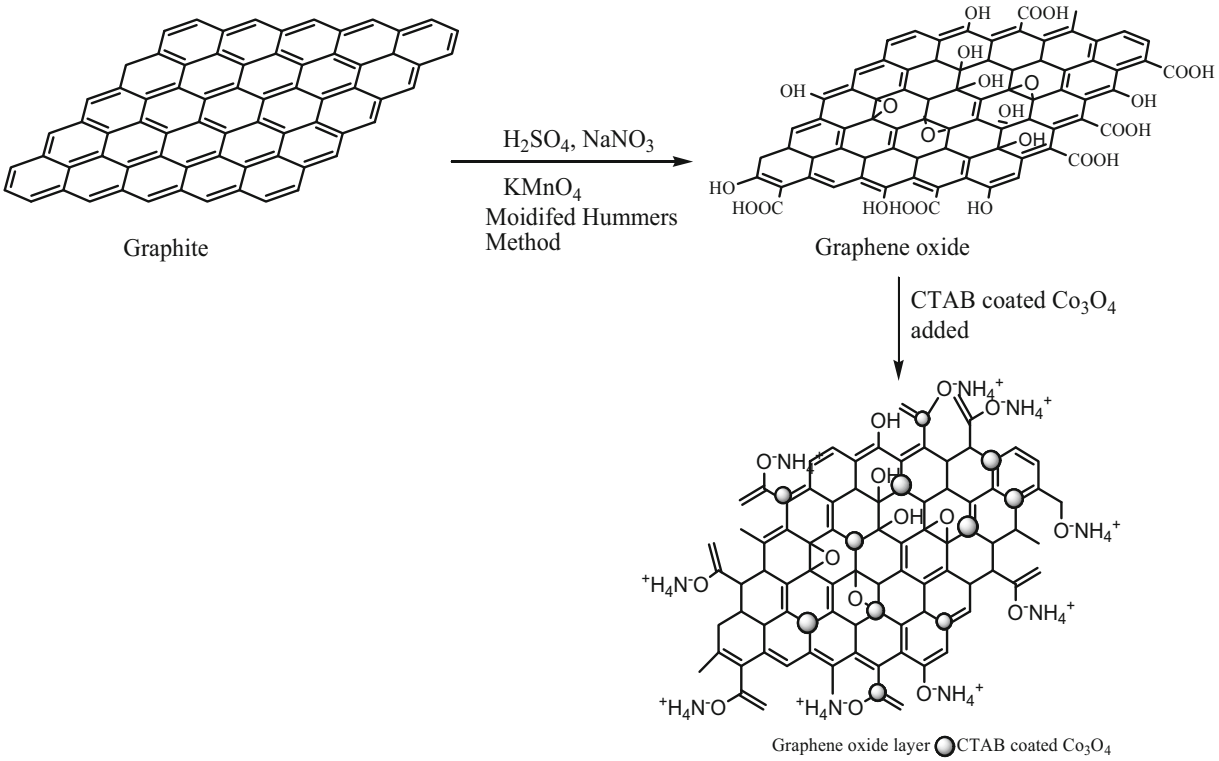

Scheme 2. Synthesis of CTAB-coated graphene oxide from graphite powder.

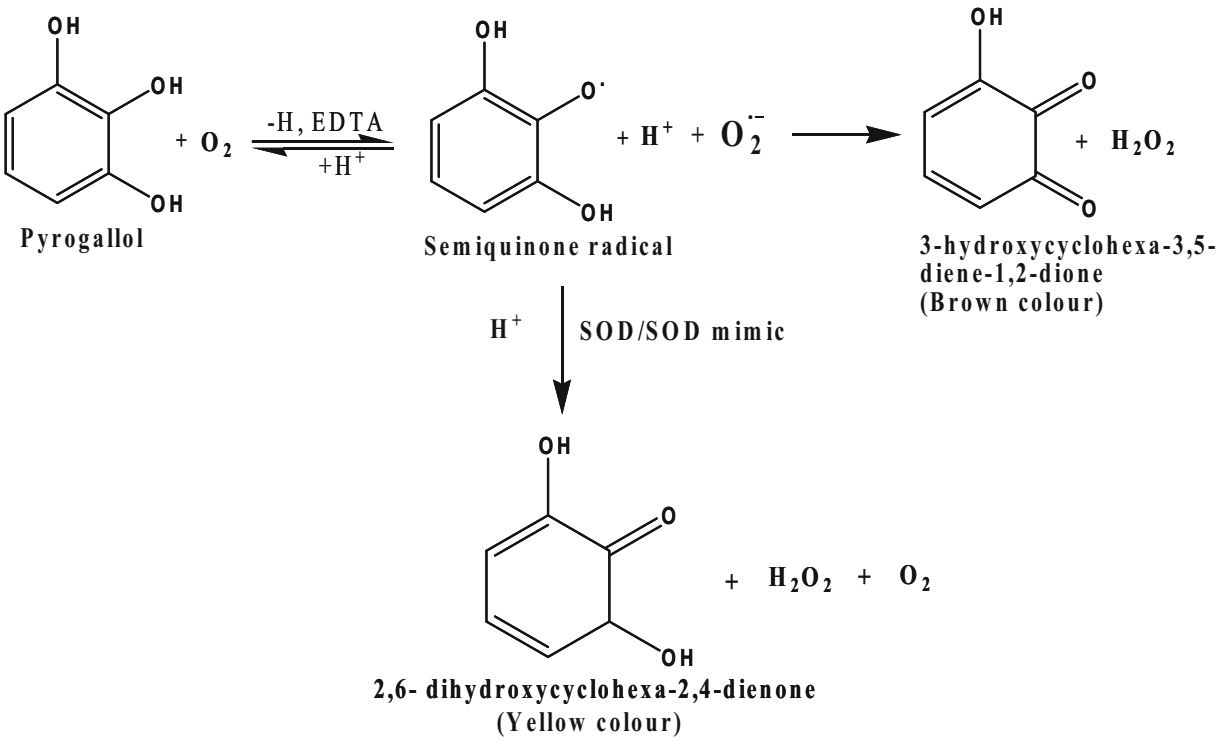

Scheme 3. Mode of action of SOD mimic.

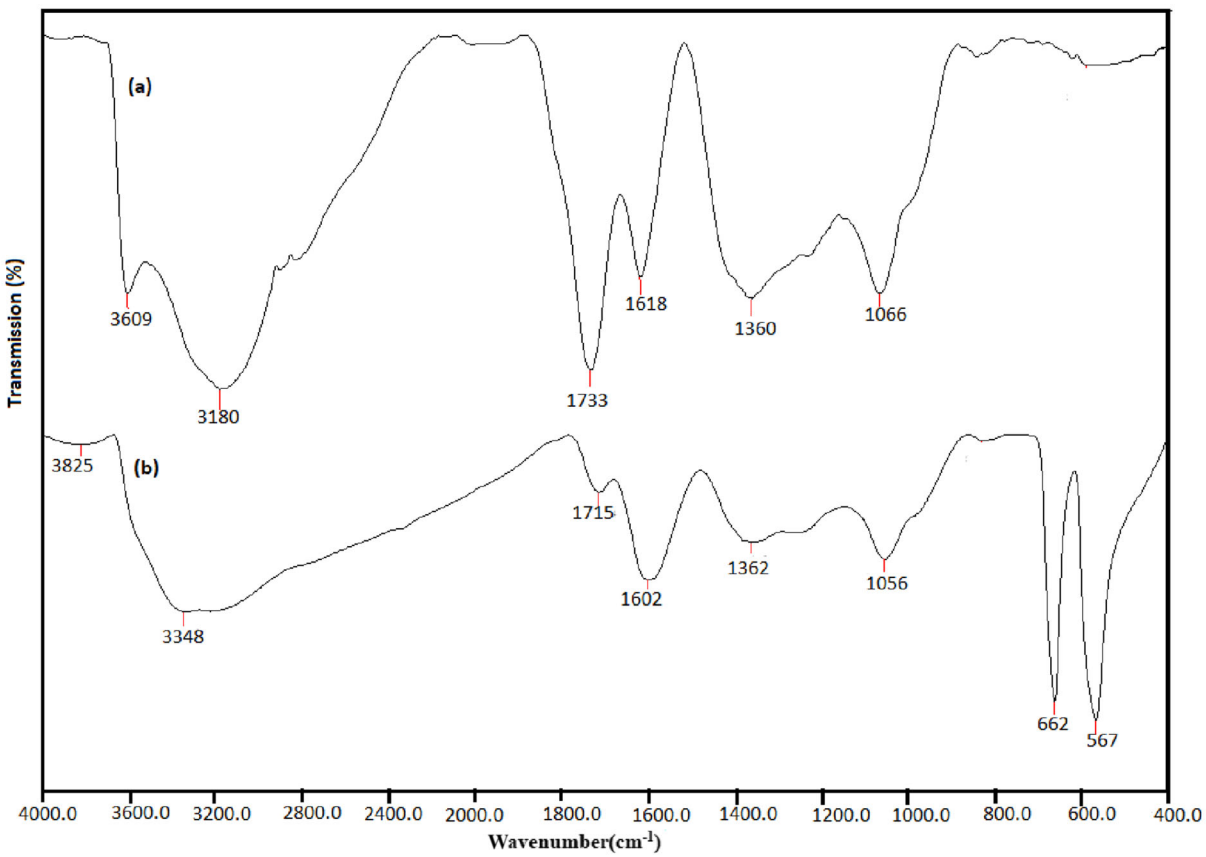

Figure 1. Fourier transform infrared spectra of (**a**) GO and (**b**) CTAB@Co_3O_4@GO NC.

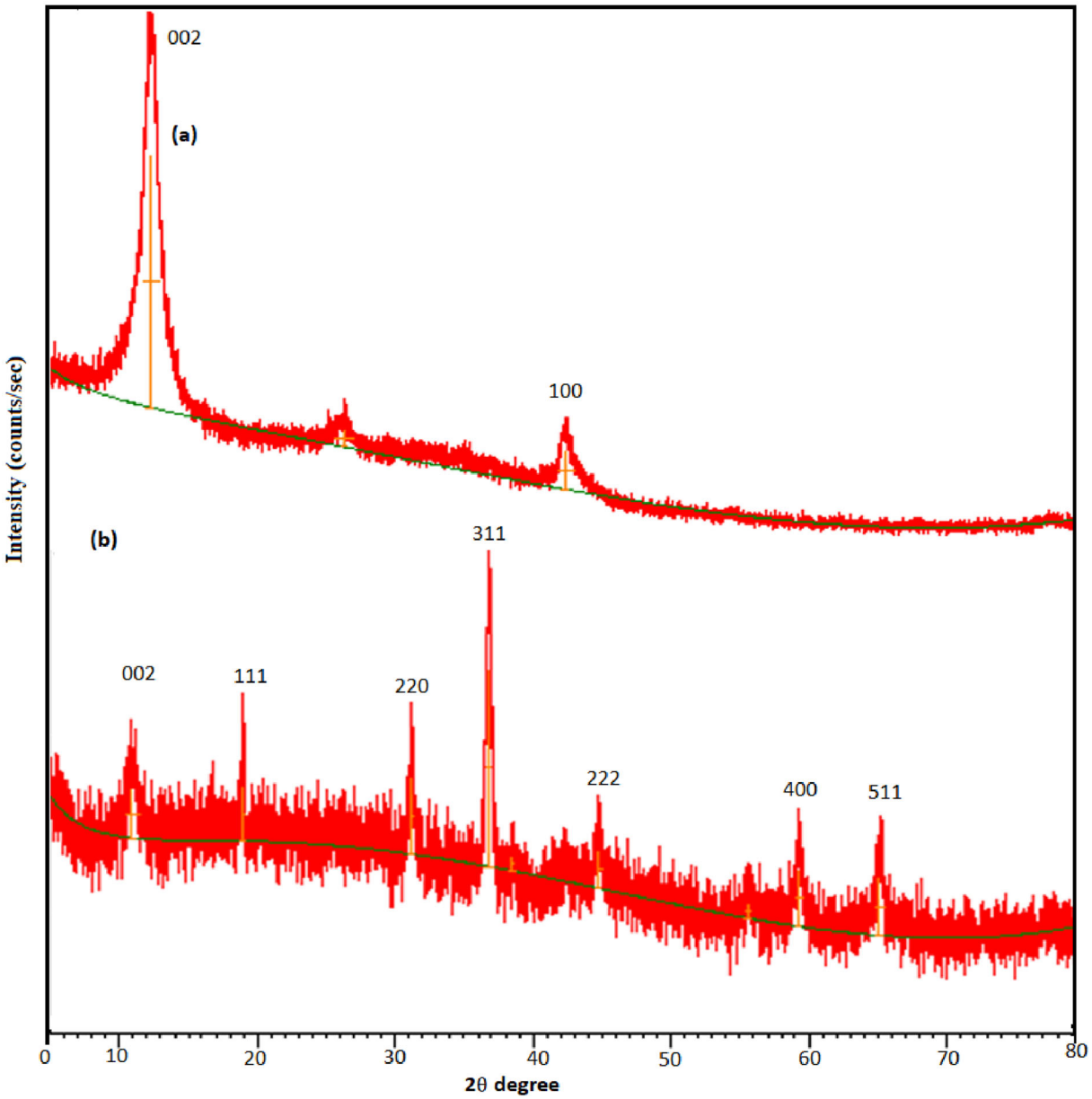

Figure 2. X-ray patterns for (**a**) GO and (**b**) CTAB@Co_3O_4@GO nanocomposite.

Table 1. Calculated XRD parameters of prepared compounds.

Nanoparticles	Lattice constant (Å)	Physical density (g cc^{-1})	Average particle diameter (nm)	d-spacing (nm)
GO	12.44	0.57	—	0.71
NC	8.07	0.01	20.0	0.24

3. Results and discussion

3.1 *Characterizations*

The Fourier transform infrared spectrum of GO (figure 1) showed bands at 3609 and 3180 cm^{-1} due to O-H stretching vibrations. The C=O of the carboxyl groups displayed stretching vibrations at 1733 cm^{-1} [27]. The bands at 1618, 1360 and 1066 cm^{-1} were assigned to the C=C skeleton vibrations, C–OH stretching vibrations and epoxy group, respectively. Nanocomposite showed the characteristic band at 567 and 662 cm^{-1}, which were assigned to Co–O

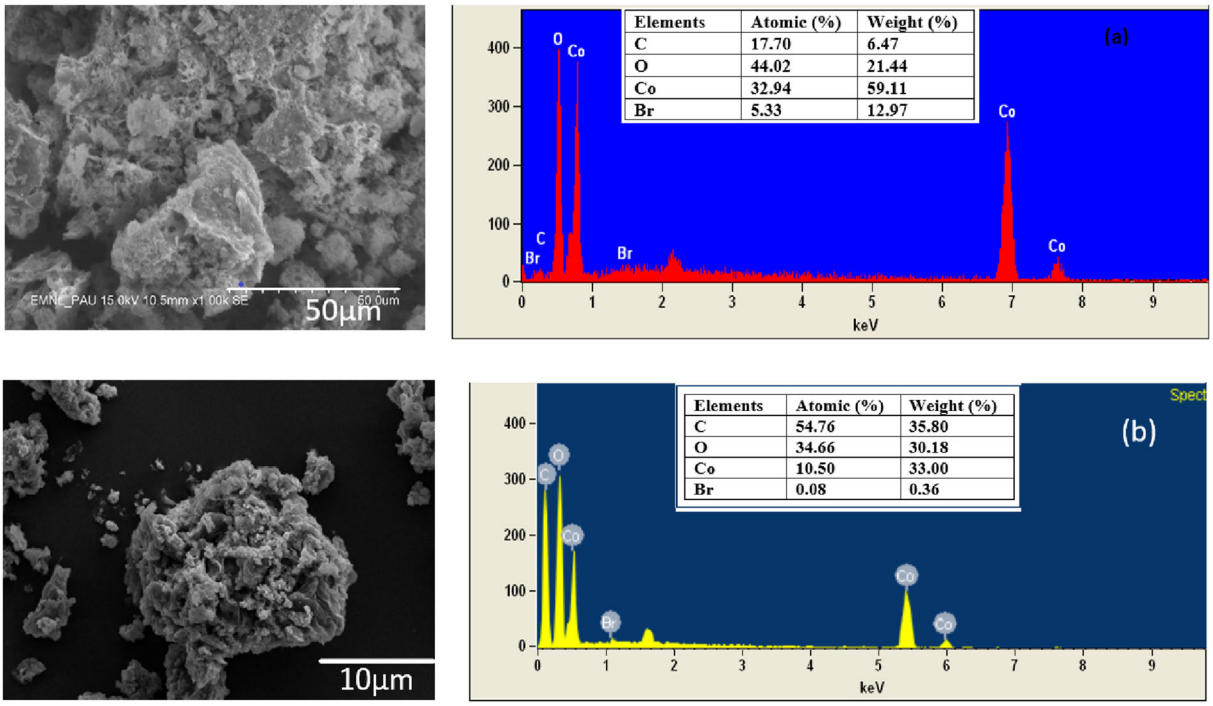

Figure 3. Scanning electron microscope–energy dispersive spectrum of (**a**) CTAB@Co_3O_4 (N-3) and (**b**) CTAB@Co_3O_4@GO nanocomposite.

stretching and O–Co–O bond bridging vibration, respectively. The band at 1602 cm^{-1} attributed to C–N bond stretching, which corresponded to the presence of CTAB in samples. NC showed a characteristic band at 3348 and 3825 cm^{-1} due to O–H stretching vibrations of bound water molecules. Bands at 1362 and 1056 cm^{-1} corresponded to C–N vibrations and epoxy groups with O–H stretching vibrations at 3348 cm^{-1}, vibrations of C=O of the carboxyl showed a red shift at 1715 cm^{-1}. C–OH stretching at 1362 cm^{-1} as compared to GO showed change in peak position, modification in C=O bonding proved presence of bonding of iron oxide NPs with GO. The Fourier transform infrared spectra of Co_3O_4 and CTAB-coated Co_3O_4 NPs are shown in supplementary figure S1. They strengthened the behaviour of CTAB and Co_3O_4 in the CTAB-coated Co_3O_4.

XRD pattern of GO showed diffraction peak at 2θ = 12.45° (002) miller plane with interplanar spacing of 0.71 nm in the layered structure of GO [27]. The d-spacing of GO verified the occupancy of oxygen containing functional groups (figure 2). XRD pattern of NC displayed peaks of both GO and Co_3O_4, thus confirming the synthesis of NC (figure 2). The relative intensity of (002) peak in case of NC was much weaker than that of GO due to its interaction with Co_3O_4. The value of d-spacing was slightly shifted from 0.71 to 0.24 nm, due to the aggregation of GO sheets [28]. The d-spacing of composites decreased in comparison to GO, which proved the Co_3O_4 were present on upper side of GO and GO sheets were aggregated. Particle size of NC decreased and its main peak sharpened. XRD parameters are shown in table 1. XRD pattern of Co_3O_4 NPs displayed 2θ at 19.10°, 31.38°, 36.94°, 38.66°, 44.91° and 55.78° having interplanar spacing of 0.46, 0.28, 0.24, 0.23, 0.21 and 0.16 nm with average particle size of 28.0 nm (supplementary figure S2). The values were further verified by matching with American Society for Testing Materials (ASTM) Data Card No. 9-418 [29]. CTAB-coated Co_3O_4 NPs showed average particle size in the range of 10–30 nm (supplementary table S1). CTAB acted as a surfactant that decreased the aggregation of Co_3O_4 NPs, hence particle size decreased. Surfactants have the effects of reducing the interfacial energy and capping of particles [30,31].

3.2 *Morphological and surface area studies*

The scanning electron microscope (SEM) micrographs depicted the morphology of NPs. Scanning electron microscope–energy dispersive spectrum patterns for the synthesized NPs are given in figure 3 and supplementary figure S3. Atomic compositions of O and Co were 13.64 and 86.36%, respectively, for Co_3O_4. EDS spectra for NCs are given in the supplementary information. Presence of C and Br gave clear evidence of the presence of CTAB in samples. SEM (figure 3) of GO depicted sheet-like structure and EDS spectrum showed carbon (65.12%) and oxygen (30.88%) and thus confirmed the ubiquity of functional groups having oxygen on the surface of GO [32]. SEM micrograph of NC is shown in figure 3. Scanning electron microscope–energy dispersive spectrum micrographs of GO and Co_3O_4 showed atomic composition of C, O, Co, Br as 54.76, 34.66, 30.50,

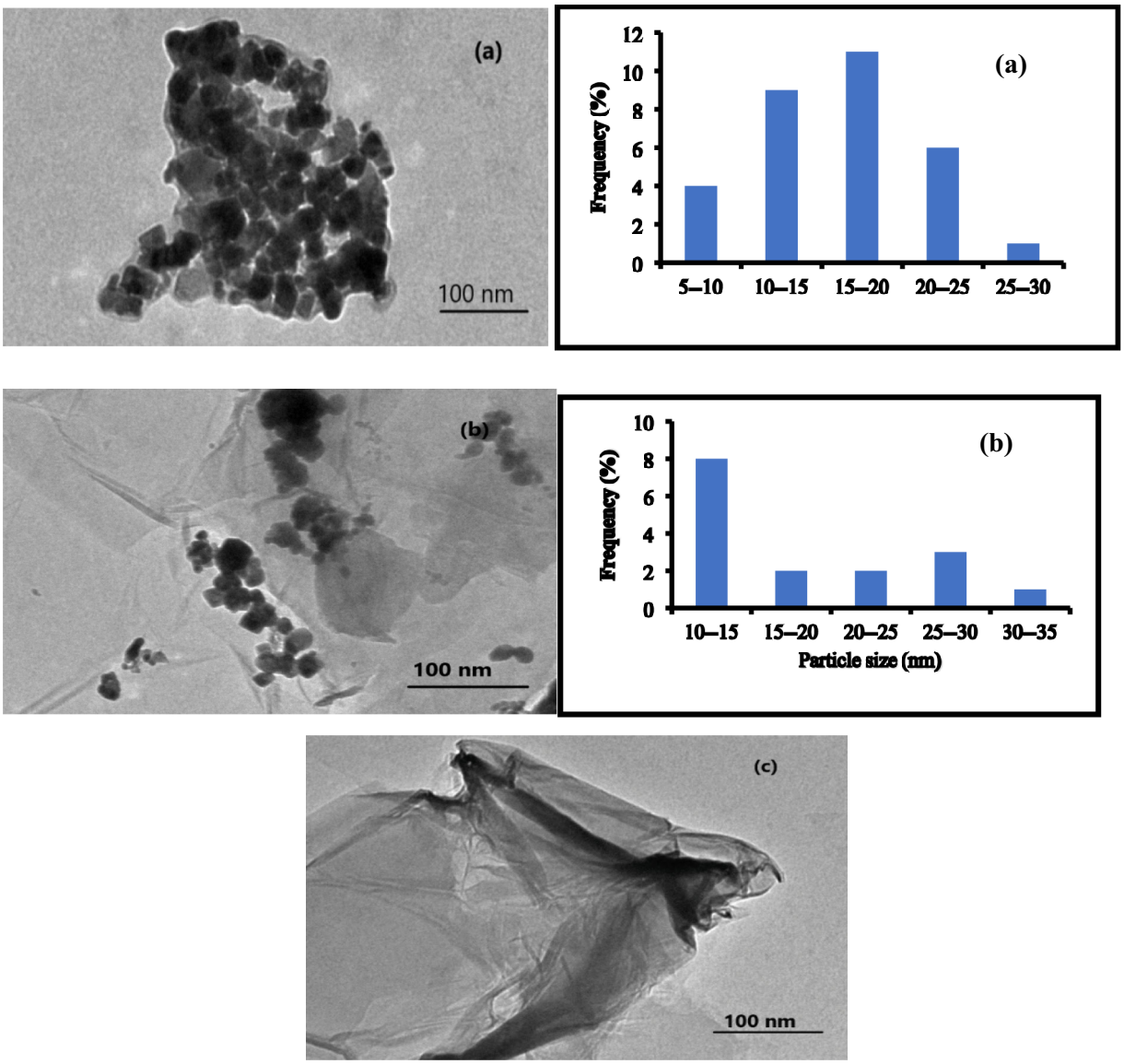

Figure 4. TEM images and histograms of (**a**) CTAB@Co_3O_4 (N-3) and (**b**) CTAB@Co_3O_4@GO nanocomposite.

0.08 and weight (%) was 35.80, 30.18, 33.00, 0.36, respectively.

TEM images of Co_3O_4 NPs in supplementary figure S4(a) showed agglomerated NPs with size in the range of 15–20 nm. Vander Waals interactions were the major reason for the agglomeration of NPs. TEM micrographs of CTAB-coated Co_3O_4 NPs depicted that on CTAB coating agglomeration was decreased, because CTAB acted as a matrix that inhibited the agglomeration of NPs. TEM histogram showed the average particle size of CTAB@Co_3O_4 NPs was in the range of 10–25 nm, respectively. TEM of GO showed number of bends and wrinkles. The double lamellar-layered structure of GO observed due to oxidation of carbon atoms in graphene layers. In the presence of Co_3O_4 NPs, GO sheets displayed multilayer agglomeration. Decrease in aggregation was observed with increase in CTAB coating due to which average particle size was decreased.

TEM image of NC in figure 4a–c showed that Co_3O_4 NPs were present on nanosheets of GO without causing damage to layers, the particle size ranged from 10 to 15 nm, which was comparable with the XRD results. Agglomeration of NPs decreased as GO provided surface to Co_3O_4 NPs. There were Vander Waals forces of attraction between GO and NPs [32]. The isotherms based on nitrogen adsorption and with pore size distribution of the NPs are depicted in figure 5 and supplementary figure S5. As per IUPAC classification, BET isotherms depicted mesoporous structures and hysteresis loops represented the H-3 type in case of Co_3O_4, CTAB@Co_3O_4 and GO. H-3 type isotherm particles reveal non-rigid clusters, which did not demonstrate adsorption at high P/P_o. NC displayed H-2 type isotherm,

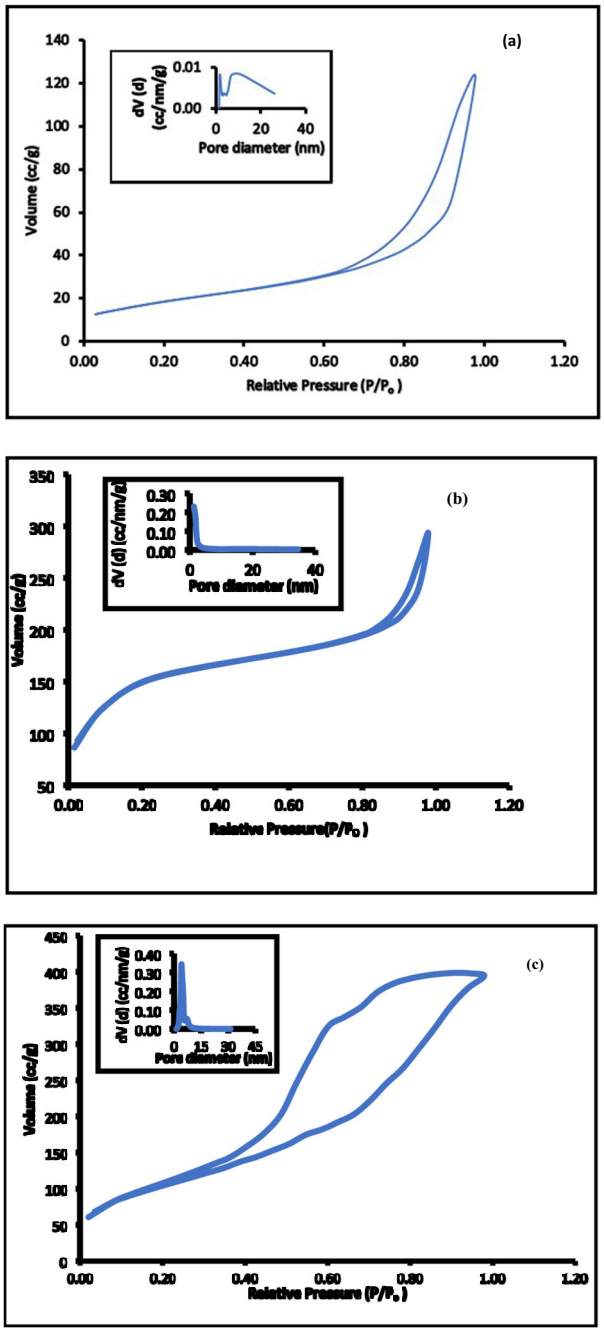

Figure 5. BET graphs of (**a**) CTAB@Co_3O_4 (N-3), (**b**) GO and (**c**) CTAB@Co_3O_4@GO nanocomposite.

Table 2. Estimated surface area, pore volume and pore diameter of prepared nanoparticles.

Nanoparticles	Surface area (m^2 g^{-1})	Pore volume (cm^3 g^{-1})	Pore diameter (nm)
N-3	60.53	0.72	2.20
GO	500.46	0.42	1.30
NC	378.19	0.68	4.10

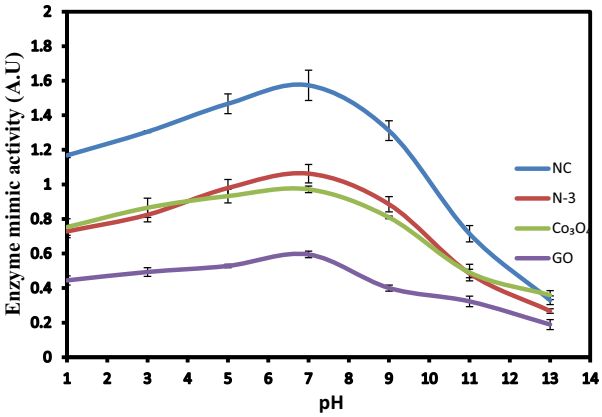

Figure 6. Effect of pH on superoxide dismutase mimic activity at 25°C using GO, CO_3O_4, CTAB@Co_3O_4 (N-3) and CTAB@Co_3O_4@GO (NC) and 1 A.U. = 50% inhibition of oxidation of pyrogallol in comparison with control.

which is usually used to describe the materials that are distorted and the distribution of pore size and shape was not well defined [33]. H-2 type of hysteresis in the NC is due to presence of Co_3O_4, CTAB and GO in it.

The Barrett-Joyner-Halenda (BJH) pore size distribution (table 2 and supplementary S2) showed small peak in bimodal distribution range of 2.0–2.2 nm in case of Co_3O_4 and CTAB-coated NPs, whereas 5 nm with unimodal distribution range in NC. The surface area and pore volume of prepared NPs are provided in table 2. The surface area of CTAB@Co_3O_4 was decreased in comparison to pristine NPs because of decreased aggregation and immobilization of CTAB onto the surface of Co_3O_4 NPs. Surface area of NC was much larger than pristine NPs because of its intercalation with GO (figure 5). The average surface area and total pore volume decreased with an increase in surfactant coatings. Surface area of NC decreased and pore volume increased in comparison to GO.

3.3 *Enzymatic studies*

Modified Marklund and Marklund method were used for enzymatic studies. Pyrogallol was used as substrate. NPs/NC/GO were used in place of SOD enzyme.

Impact of pH variation on the enzyme mimic activity of NPs was studied in the pH range of 1.0–14.0 at 25°C (figure 6). pH 8.0 was found to be the optimum pH for NPs. The reason for the decreased activity was due to the increased alkalinity of the medium, which tends to aggregate these NPs resulting in the reduction of surface/volume ratio. Guzman *et al* [34] and Loosli *et al* [35] have reported similar trend in the colloidal stability of TiO_2. Ardizzone *et al* [36] also described the zero-point charge of Co_3O_4. NC showed best activity at optimum pH followed by N-3, pristine NPs and GO, respectively. Activity of GO was very less at this pH but the composite showed best activity

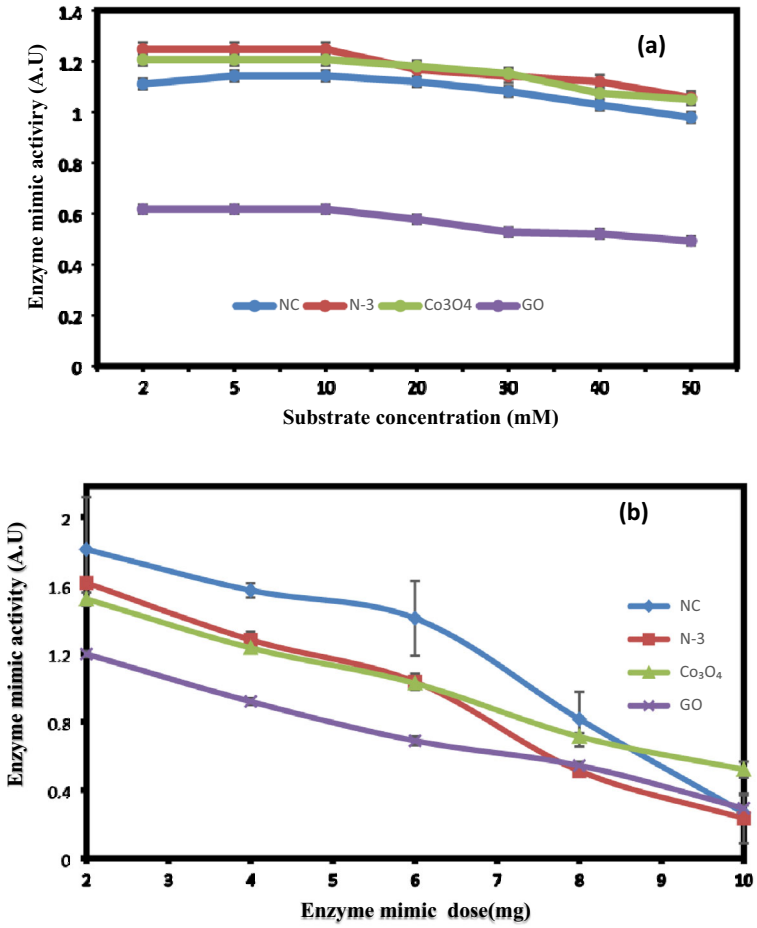

Figure 7. (**a**) Effect of substrate concentration on superoxide dismutase mimic activity at 25°C using GO, Co_3O_4, CTAB@Co_3O_4 (N-3) and CTAB@Co_3O_4@GO (NC). (**b**) Effect of enzyme mimic dose on the superoxide dismutase mimic activity using GO, CO_3O_4, N-3, NC with substrate 10 mM and 1 A.U. = 50% inhibition of oxidation of pyrogallol in comparison with control.

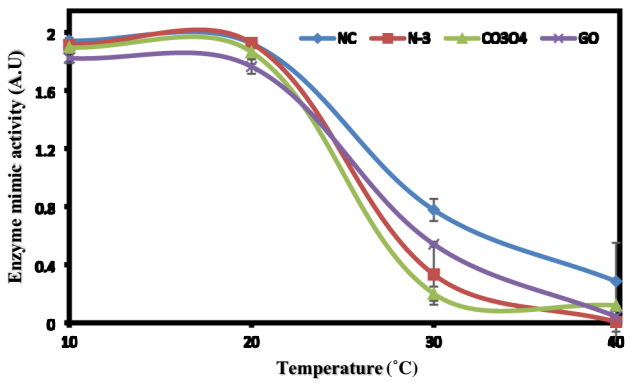

Figure 8. Effect of temperature on superoxide dismutase mimic activity using GO, Co_3O_4, CTAB@Co_3O_4 (N-3) and CTAB@Co_3O_4@GO (NC) with substrate 10 mM and 1 A.U. = 50% inhibition of oxidation of pyrogallol in comparison with control.

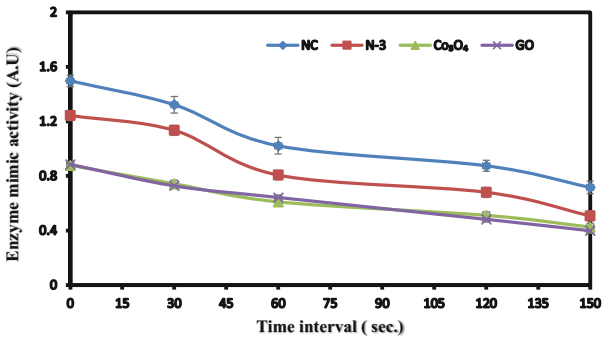

Figure 9. Contact time for CTAB@Co_3O_4@GO (NC), CTAB@Co_3O_4 (N-3), Co_3O_4 and GO at 10 mM of substrate concentration and 1 A.U. = 50% inhibition of oxidation of pyrogallol in comparison with control.

because of π–π interactions between substrate and GO, which played major role to increase the substrate adsorption on Co_3O_4 NPs. This means that SOD mimic activity of Co_3O_4 NPs was increased as Co_3O_4 acted as catalytic centres and GO sheets provided platform for dispersal of

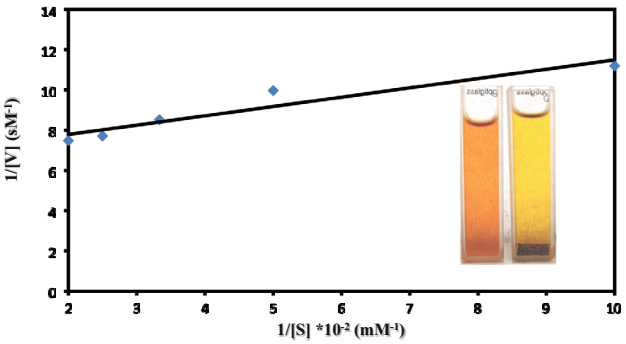

Figure 10. Lineweaver–Burk plot for NC.

CTAB@Co_3O_4 NPs in the NC, which led to increase in its catalytic activity by the synergistic effect.

Substrate concentration was studied between 2 and 40 mM (figure 7, supplementary table S4). All enzyme mimics showed best activity up to 10 mM of pyrogallol concentration. With an increase in the concentration of substrate up to 10 mM, its oxidation by superoxide radical anions was decreased due to SOD mimic activity of NPs/NC, which led to the observed increase in SOD mimic activity. On increasing the substrate concentrations, the observed decrease in SOD mimic activity can be ascribed to autooxidation of pyrogallol. Li [37] observed that below 40 mM no linear relationship was observed for pyrogallol oxidation. With the increase in concentration of pyrogallol, free radicals also increased, due to which it became difficult for enzyme mimic to oxidize all the radicals and its activity decreased. Effect of NPs dose was tested by the addition of enzyme mimic (2–10 mg) in the reaction mixture. The activity decreased with increase in the dose of enzyme mimic because of availability of more active sites at low concentration than at high concentration due to agglomeration of NPs (figure 7b).

The temperature was varied from 10 to 40°C. The maximum SOD mimic activity was observed at 20°C by the NC followed by CTAB@Co_3O_4, Co_3O_4 and GO (supplementary table S5). The reaction rate increased up to 20°C and with further increase in temperature, the reaction rate decreased, indicating that 20°C was the optimum temperature for SOD mimic activity of NPs/NC. The diminished activity following the optimum temperature was due to the wreckage of bonds within NPs/NC and substrate, as weakening of bonds of metal complex occurs with increase in temperature, due to which the interaction of NPs with substrate was decreased (figure 8). π–π interactions exist between substrate and NPs, which also decreases with increase in temperature. Among NPs/GO and NC, the NC retained maximum activity (0.8 AU) at 30°C indicating the effectiveness of NC (supplementary table S6). Impact of contact time (figure 9) on SOD mimic activity was studied for 150 s by taking reading at interval of 30 s. As contact time increased the oxidation of substrate also increased, as superoxide radical anions are continually formed in the presence of environmental O_2. Thus, the activity of NPs/NC decreased with increase in contact time (supplementary table S7). However, in the absence of NPs/NC the oxidation of pyrogallol was instantaneous. However, the enzyme mimics slowed down the process of autooxidation. As exposure time of pyrogallol to the environmental oxidation was increased, the activity of enzyme mimics decreased. Maximum activity was observed at 30 s and minimum at 150 s. NC was more effective than pristine and CTAB-coated NPs even after 150 s of contact time, whereas GO exhibited minimum activity. The NC had activity of 1.0 AU after 150 s, which corresponds to 50% inhibition of pyrogallol autooxidation, thus showing its effectiveness in scavenging superoxide radicals and its role as a promising SOD mimic.

3.4 *Steady-state enzyme kinetics*

The SOD mimic activity of NC was examined by calculating steady-state kinetic parameters of reaction using different pyrogallol concentrations. The calculated K_m and V_{max} values of the NCs was 0.0675 mM and 0.146 mol s^{-1}, respectively (figure 10). These values were compared with values of artificial enzyme mimics given in literature [38–41], as natural SOD and NC showed activities at

Table 3. K_m and V_{max} values of reported SOD mimics.

K_m (mM)	V_{max}	New enzyme/enzyme mimic	References
0.0752	—	Iron phosphate microflowers	[8]
2.7	—	Carbon anti-oxidant nanozymes	[38]
4.20	0.77 mol s^{-1}	$CuFe_2O_4$ NPs	[39]
10.16×10^3	—	CuZn SOD (*Cicer arietinum*)	[40]
264.8	2.461×10^6 mol s^{-1}	SOD Cl	[40]
47×10^3	1250 ± 24 Units per mg of protein	CuZn SOD (*Curcuma aromatica*)	[41]
0.0675	0.1456 mol s^{-1}	Present study	

different pH comparison with SOD and SOD mimics (table 3). Although natural enzymes showed lower K_m and higher V_{max} values, but K_m value of NC is lower and V_{max} value is higher than reported SOD mimics, which correspond to good SOD mimic activity of the synthesized NC. The advantage of synthesized SOD mimic over natural enzyme is ease of synthesis, stable nature and easy storage.

Statistical analysis results are presented in supplementary tables S3–S7. The contrast is considered important when $P \leq 0.05$. All the results are significant and error was in the range of 0.005–0.140. The statistical analysis authenticated the observed experimental results.

4. Conclusion

Mechanism of the reaction is given in scheme 3. The pyrogallol reacts with oxygen to produce superoxide radical anions, which catalyse its autooxidation, thus leading to formation of semiquinone radical. However, in the presence of NC the superoxide radical anions are dismutated and scavenged by the NCs and are converted into H_2O_2. Removal of superoxide radical anions, inhibited autooxidation of pyrogallol, which was clearly evident by the lowering of absorbance of the solution of pyrogallol in the presence of NCs, as enzyme mimic as compared to the control, which was pyrogallol alone in the absence of enzyme mimic.

The SOD mimic activity of Co_3O_4 NPs CTAB@Co_3O_4 NPs, GO and their NC, i.e., CTAB@Co_3O_4@GO was comparatively analysed and summarized. The NC had enhanced SOD mimic activity as compared to pristine NPs or CTAB@Co_3O_4 NPs. CTAB coating helped in increasing the surface area and interaction of NPs with the substrate, whereas GO provided matrix and played synergistic role in enhancing the SOD mimic activity. Lower values of Michaelis constant K_m, as compared to reported SOD mimics authenticates its superiority as enzyme mimic. The CTAB@Co_3O_4@GO NC has great potential to substitute SOD enzyme-based assay, due to its stability, which is the major drawback in handling natural SOD enzyme.

References

[1] Policar C 2016 in *Redox-active therapeutics* (New Jersey: Humana Press) p 125

[2] Goto J J, Zhu H, Sanchez R J, Nersissian A, Gralla E B, Valentine J S *et al* 2000 *J. Biol. Chem.* **275** 1007

[3] Kuah E, Toh S, Yee J, Ma Q and Gao Z 2016 *Chem. A Eur. J.* **22** 8404

[4] He W, Wamer W, Xia Q, Yin J J and Fu P P 2014 *J. Environ. Sci. Heal.–Part C Environ. Carcinog. Ecotoxicol. Rev.* **32** 186

[5] Singh N, Kumar S K, Geethika M and Mugesh G 2021 *Angew. Chem.–Int. Ed.* **60** 3121

[6] Nikolopoulou S G, Boukos N, Sakellis E and Efthimiadou E K 2020 *J. Inorg. Biochem.* **211** 111177

[7] Barbanente A, Palazzo B, Esposti L D, Adamiano A, Iafisco M, Ditaranto N *et al* 2021 *J. Inorg. Biochem.* **215** 111334

[8] Wang W, Jiang X and Chen K 2012 *Chem. Commun.* **48** 7289

[9] Fedorenko S V, Grechkina S L, Mukhametshina A R, Solovieva A O, Pozmogova T N, Miroshnichenko S M *et al* 2018 *J. Inorg. Biochem.* **182** 170

[10] Qu K, Shi P, Ren J and Qu X 2014 *Chem.–A Eur. J.* **20** 7501

[11] Xong Y, Qin Y, Su L and Ye F 2017 *Chem.–A Eur. J.* **23** 11037

[12] Korsvik C, Patil S, Seal S and Self W T 2007 *Chem. Commun.* **2007** 1056

[13] Dong J, Song L, Yin J J, He W, Wu Y, Gu N *et al* 2014 *ACS Appl. Mater. Interfaces* **6** 1959

[14] Xiao F, Song J, Gao H, Zan X, Xu R and Duan H 2012 *ACS Nano.* **6** 100

[15] Bai S, Shen X, Zhu G, Xu Z and Yang J 2012 *Cryst. Eng. Comm.* **14** 1432

[16] Wang Z, Chen M, Shu J and Li Y 2016 *J. Alloys Compd.* **682** 432

[17] Song L, Huang C, Zhang W, Ma M, Chen Z and Gu N 2016 *Colloids Surf. A Physicochem. Eng. Asp.* **506** 747

[18] Li L, Zeng C, Ai L and Jiang J 2015 *J. Alloys Compd.* **639** 470

[19] Singh N, Savanur M A, Srivastava S, D'Silva P and Mugesh G 2017 *Angew. Chem.–Int. Ed.* **56** 14267

[20] Singh G, Kushwaha A and Sharma M 2020 *J. Alloys Compd.* **825** 154134

[21] Ragg R, Schilmann A M, Korschelt K, Wieseotte C, Kluenker M, Viel M *et al* 2016 *J. Mater. Chem. B* **4** 7423

[22] Khalid H, Hanif M, Hashmi M, Mahmood T, Ayub K and Monim-ul-Mehboob M 2013 **13** 1944

[23] Asati A, Santra S, Kaittanis C, Nath S and Perez J M 2009 *Angew. Chem.–Int. Ed.* **48** 2308

[24] Zhang Q A, Wang X, Song Y, Fan X H and Martín J F G 2016 *J. AOAC Int.* **99** 504

[25] Zhao G, Ren X, Gao X, Tan X, Li J, Chen C *et al* 2011 *Dalt. Trans.* **40** 10945

[26] Marklund S and Marklund G 1974 *Eur. J. Biochem.* **47** 469

[27] Luo W, Li Y S, Yuan J, Zhu L, Liu Z, Tang H *et al* 2010 *Talanta* **81** 901

[28] Hakimi M, Alimard P and Yousefi M 2014 *Ceram. Int.* **40** 11957

[29] Jung H N R, Han W, Cho H H and Park H H 2017 *Mater. Express.* **7** 291

[30] Gopalakrishnan A, Krishnan R, Thangavel S, Venugopal G and Kim S J 2015 *J. Ind. Eng. Chem.* **30** 14

[31] Baláž P 2008 (eds) *Mechanochemistry in nanoscience and minerals engineering* (Materials) p1. https://doi.org/10.1007/978-3-540-74855-7

[32] Menchaca-Campos C, García-Pérez C, Castañeda I, García-Sánchez M A, Guardián R and Uruchurtu J 2013 *Int. J. Polym. Sci.* **2013** https://doi.org/10.1155/2013/621618

[33] Alothman Z A 2012 *Materials (Basel)* **5** 2874

[34] Guzman K A D, Finnegan M P and Banfield J F 2006 *Environ. Sci. Technol.* **40** 7688

[35] Loosli F, Le Coustumer P and Stoll S 2013 *Water Res.* **47** 6052

[36] Ardizzone S, Spinolo G and Trasatti S 1995 *Electrochim. Acta* **40** 2683
[37] Li X 2012 *J. Agric. Food Chem.* **60** 6418
[38] Wu G, Berka V, Derry P J, Mendoza K, Kakadiaris E, Roy T *et al* 2019 *ACS Nano.* **13** 11203
[39] Verma V, Kaur M and Sharma S 2019 *Bull. Mater. Sci.* **42** 1
[40] Kumar A, Kaachra A, Bhardwaj S and Kumar S 2014 *Process Biochem.* **49** 1288
[41] Utami R A, Asyarie S and Retnoningrum D S 2018 *J. Appl. Pharm. Sci.* **8** 115